Materials Science & Engineering A 832 (2022) 142510

Contents lists available at ScienceDirect

Materials Science & Engineering A

journal homepage: www.elsevier.com/locate/msea

# Microstructure and mechanical behaviors of Al/Cu laminated composites fabricated by accumulative roll bonding and intermediate annealing

Runrun Xu [1], Ningning Liang [1], Limin Zhuang, Dajie Wei, Yonghao Zhao [*]

*Nano and Heterogeneous Materials Center, School of Materials Science and Engineering, Nanjing University of Science and Technology, Nanjing, 210094, Jiangsu, PR China*

ARTICLE INFO

*Keywords:*
Laminated composites
Accumulative roll bonding
Annealing
Interface
Microstructure
Mechanical properties

ABSTRACT

Strength and toughness of laminated composites with alternatively stacked "brick-and-mortar" structure can be synchronously improved along the direction parallel to the layer interface. However, it is still a challenge to prepare high-performance laminated composites in large quantities to meet industrial needs. In this work, we employ accumulative roll bonding (ARB) and/or intermediate annealing to prepare Al/Cu laminated composites as cheaper substitutes for Cu alloys due to lightweight and considered electrical conductivity. Our results show that the ARB process decreases the layer thicknesses and grain sizes, and improves the Vickers micro-hardness of Al/Cu laminated composites. As the ARB cycle increases from 1 to 8, the tensile strength firstly increases from 279.20 MPa to 358.71 MPa, and then decreases to 317.88 MPa. Meanwhile, the uniform elongation firstly increases from 1.25% to 1.71%, and then decreases to 0.58%. These variations of tensile properties are tightly linked to the layer-integrity and microstructures of Al and Cu layers. Moreover, the intermediate annealing (350 °C for 30 min) applied after every 2 ARB cycles can significantly increase the tensile strength, uniform elongation and elongation to failure, especially for Al/Cu laminated composites with high ARB cycles, because intermediate annealing remarkably improves the interfacial metallurgical bonding and continuity/integrity of Al and Cu layers. However, the final annealing for long time would introduce brittle intermetallics (like AlCu and $Al_2Cu$), and therefore deteriorate the tensile ductility. This work provides a new treatment process for fabricating Al/Cu laminated composites with synchronously increasing strength and ductility.

## 1. Introduction

The development of science and technology puts forward a variety of performance requirements for service materials. However, these needs cannot be easily met at the same time for materials with single phase or constituent. One economical solution is to design composites by altering constituents and/or their morphology, like particle- and fiber-reinforced composites as well as laminated composites [1–3]. The strength and toughness of the laminated composites can be synchronously improved along the direction parallel to the layer interface, whereas the strength is enhanced with the cost of toughness along the normal direction of the layer interface. Such a strong anisotropy of laminated composites is beneficial for cost-saving and weight-saving of materials with anisotropic service performance. Up to date, numerous laminated composites, featuring alternating stacked hard and soft layers with sharp interfaces, have been synthesized, such as Ti/Al [4–11].

Since Tsuji et al. [12] developed the ARB method, it has been widely used to fabricate bulk nanocrystalline, ultrafine-grained metals and laminated composites for the superiority of low cost and high production efficiency. Gao et al. [13] fabricated barcode-like Cu/Nb nanolaminates via modified ARB, which present excellent oxidation resistance, moderate ductility and undamaged superconductivity. Not only mechanical properties but also microstructure would be alternated during ARB, such as texture and phase constituents [14–16]. Wang et al. [17] found that some unexpected brittle intermetallics were introduced during ARB of Mg–Li–Al/Al–Li composites. Such variations obviously have an impact on the performance of metallic laminated composites. Thus, it is crucial to investigate the microstructure evolutions during ARB of dissimilar metals to understand the properties and guide designation.

Al/Cu laminated composites are considered as cheaper substitutes for Cu alloys because of their lightweight and considered electrical

* Corresponding author.
*E-mail address:* yhzhao@njust.edu.cn (Y. Zhao).
[1] These authors contributed equally.

https://doi.org/10.1016/j.msea.2021.142510
Received 16 September 2021; Received in revised form 5 December 2021; Accepted 11 December 2021
Available online 14 December 2021

conductivity. Eizadjou et al. [18] investigated the microstructure and mechanical properties of Al/Cu laminated composites. They found that the fragment of Cu layers is the main cause for the increase of strength and decrease of ductility. Wang et al. [19] reported that the grain size and thickness of diffusion layer are main determinants for mechanical properties of Al/Cu laminated composites. Yu et al. [20] claimed that the initial microstructure, including grain size, crystal orientation, and interface constraint are major determinants for plastic deformation of Al/Cu laminated composites. Vahid et al. [21] found that both textures in Al and Cu layers are transformed during ARB of Al/Cu laminated composites. By adjusting microstructure parameters of the component materials including layer thickness and interfacial configuration, one may obtain desired properties satisfying different industrial requirements. However, there still exists an question for the time being. Is it the layer-integrity or microstructure characteristics that determine the strength and ductility during ARB of Al/Cu laminated composites? Moreover, except for the above few papers, there is no systematic and in-depth study to reveal microstructure evolutions of Al and Cu layers during ARB.

Considering the asynchrony of plastic flow during ARB of dissimilar metals, annealing is an economical route to improve mechanical properties (like ductility) of ARB-processed laminated composites [22,23]. However, the bonding interface might be unstable during annealing. Hsieh et al. [24] found that pre-annealing remarkably promotes the formation of $Al_2Cu$, $Al_4Cu_9$, and AlCu when Al/Cu laminated composites ARB-processed at 300 °C. Tayyebiet al. [25] acclaimed that $Al_4Cu_9$–$Al_3Cu_4$–AlCu–$Al_2Cu$ intermetallic layer is formed at the bonding interface of Al/Cu laminated composites after ARB and final annealing. These intermetallics increase the micro-hardness, but harm the ductility of Al/Cu laminated composites [26,27]. Up to now, the influence of intermediate annealing is less reported, let alone for the comprehensive influence of intermediate annealing and final annealing. However, they might be essential for fabricating Al/Cu laminated composites.

In the present work, two routes, ARB and ARB + intermediate annealing were adopted to fabricate Al/Cu laminated composite. The microstructure of the Al/Cu laminated composites was deeply investigated via scanning electron microscopy (SEM), energy dispersive spectrum (EDS) and transmission electron microscopy (TEM) techniques. Moreover, the micro-hardness, tensile properties and fracture surfaces were investigated. Finally, the comprehensive influence of intermediate annealing and final annealing was also investigated.

## 2. Materials and experimental procedures

Commercial pure Al sheets supplied for the present work were cold-rolled AA1100 sheets with a thickness of 1 mm, and the chemical composition of Al-0.55Fe-0.03Si-0.0123Mg-0.0123Mn-0.01Cu-0.01Ti-0.01V-0.0007Ni-0.0002B (wt %). Oxygen-free Cu sheets were also processed by cold rolling before ARB process, with the thickness of 2 mm and the chemical composition of Cu-0.004Al-0.004Zn-0.0006Pb-0.0004P-0.0003Fe (wt %).

Al/Cu laminated composites were fabricated by ARB, as illustrated in Fig. 1. The cold-rolled Al and Cu sheets were firstly cut into cuboids with the length of 150 mm and the width of 25 mm, then annealed in a vacuum tube furnace for 2 h. The annealing temperatures for Al and Cu sheets were 370 °C and 480 °C, respectively. The annealed cuboids were then socked in acetone for 0.5 h, stacked alternately and fixed by four rivets. After that, the stacked cuboids were synchronously cold-rolled at room temperature without preheating or lubrication. In each rolling cycle, the rolling speed was 0.34 m $s^{-1}$ and the thickness reduction was 50%. Moreover, some Al/Cu laminated composites were fabricated with ARB and intermediate annealing (termed as "ARB + intermediate annealing"). That is, the Al/Cu laminated composites were firstly ARB-processed for 2 cycles, then annealed at 350 °C for 30 min in vacuum and air-cooled to ambient temperature, and then continued ARB process for another 2 cycles following annealing. Subsequent processing is also handled according to the above cycle. Through these steps (Fig. 1), Al/Cu laminated composites with 1–8 cycles were obtained.

The microstructure and layer morphology of Al/Cu laminated composites were observed on a Zeiss Auriga focused ion beam (FIB)/SEM crossbeam system. Before the SEM observation, Al/Cu laminated composites were manually ground and afterward polished via a Buehler ElectroMet 4 electrolytic polisher. The TEM observation was performed on an FEI Tecnai 20 TEM at the operating voltage of 300 kV. Specimens for TEM observation were prepared through the following steps. Firstly, slices with a thickness of ~0.5 mm were cut from Al/Cu laminated composites along the RD-ND (RD and ND represent the rolling direction and nominal direction, respectively) plane. Then, the slices were mechanically ground to foils with a thickness of ~40 μm. Finally, these foils were thinned to a thickness through which an electron beam can penetrate via a Gatan 695 precision ion polishing system.

The hardness of Al/Cu laminated composites was measured on RD-TD (TD represents the transverse direction) and RD-ND planes via an HMV-G21 DT micro-Vickers sclerometer at room temperature with an indentation time of 15 s. The applied loads were 25 g and 50 g for Al and Cu layers, respectively. For high measurement accuracy, 18 indentation marks were made on each plane of Al/Cu laminated composites. Uniaxial tensile tests were carried out on a walter + bai LFM testing machine at ambient temperature with the tensile rate of 0.5 mm $min^{-1}$. Tensile specimens were electro-spark machined into dog-bone shape, with the gauge dimensions of 15 mm × 2 mm × 1 mm from the middle of Al/Cu laminated composites along the RD direction. Each tensile sample is repeated at least once. The fracture surface of tensile specimens was observed on an FEI Quanta 250F SEM at the operating voltage of 10 kV.

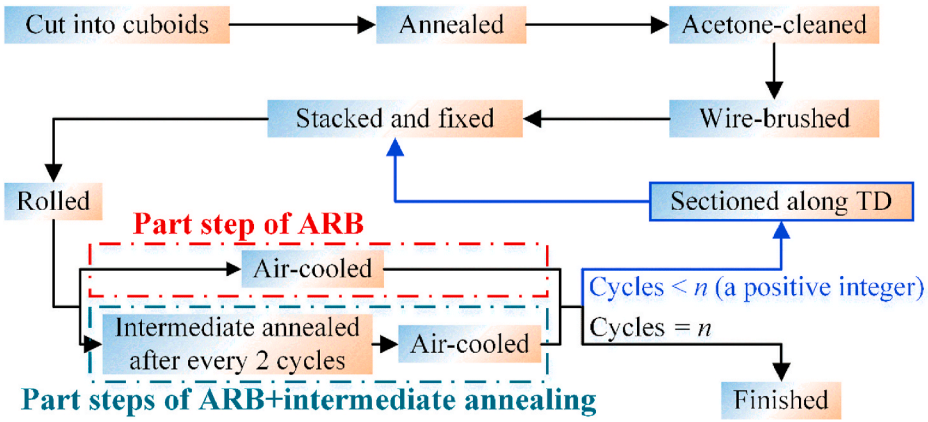


**Fig. 1.** ARB procedures for fabricating Al/Cu laminated composites.

## 3. Results

### 3.1. Microstructure and morphology of Al and Cu layers

Fig. 2 shows microscopic morphologies of ARB-processed Al/Cu laminated composites. Fig. 3 shows the quantitative changes of the Al and Cu layer thickness against the ARB cycle, which were obtained via calculating the average length of ten equidistant line segments intercepted by the Al/Cu interface. As seen from Figs. 2 and 3(a)–(b), when the ARB cycle increases from 1 to 6, the Al layer thickness decreases from initial 465.40 μm to 13.24 μm, and the Cu layer thickness decreases from 916.20 μm to 28.06 μm. Moreover, at the beginning ARB stage with 1–3 ARB cycles (Fig. 2(a)–(b) and Fig. 3), both Al and Cu layers have uniform thicknesses with small waves and straight Al/Cu interfaces, indicating that the stress and strain are uniformly distributed along the RD direction. However, when the ARB cycle is 5, the thicknesses of Al and Cu layers become non-uniform and the Al/Cu interfaces are not flat, but undulating, as shown in Fig. 2(c). Nevertheless, the laminated Al/Cu structure of alternate stacking is still intact and continuous in most cases. When increasing the ARB cycle up to 6, shear deformation takes place along the direction with an angle of ~22° deviating from the RD direction (Fig. 2(d)). As a result, both initially continuous Al and Cu layers gradually fragment and become non-continuous. Moreover, the shear deformation makes adjacent Al layers touch together, forming Al/Cu network structure deviated from the horizontal direction. It is obvious that shear stress might play a significant role in the fragmentations of Al and Cu layers.

Fig. 4 presents the magnified FIB/SEM images near Al/Cu interfaces of the ARB-processed Al/Cu laminated composites. Note that only one FIB/SEM image (Fig. 4(a)) is displayed when the ARB cycle is 1, because the Al/Cu laminated composite in this case only contains one Al/Cu interface. As seen from Fig. 4(a)–(e), there exists a gap with several hundred nanometers between Al and Cu layers after 1 ARB cycle. The reliable interfacial metallurgical bonding between Al and Cu layers gradually achieves when the ARB cycle increases to 3 and 6.

Fig. 5 shows the microstructure of Al and Cu layers in the Al/Cu laminated composites with 1–6 ARB cycles. As seen from Fig. 5(a)–(f), elongated grains with the thickness of about 0.65 μm were formed in Al layers after 1 ARB cycle. The elongated Al grains become equiaxed and are further refined gradually below 0.50 μm with increasing ARB cycle. Different from the microstructure evolution of Al layers, grains in Cu layers are always in the shape of long strips. The thickness of strip-like Cu grains decreases gradually from 0.55 μm to less than 0.13 μm when increasing the ARB cycle from 1 to 6. Under the same deformation conditions, the thickness of strip-like Cu grains is smaller than the grain size of Al layers. The above different microstructural evolutions of Al and Cu layers indicate that various metallurgical phenomena, like recovery and recrystallization occurred in ARB-processed Al/Cu laminated composites.

The microstructures especially dislocations in the ARB-processed Al/Cu laminated composites are further characterized by TEM observation, as shown in Fig. 6. TEM results further verified the above microstructure evolutions in Al and Cu layers. As seen from Fig. 6(a), strip-like dislocations cells (as pointed by white arrows) are formed in the Al layers after 1 ARB cycle, and selected area electron diffraction (SEAD) pattern with arc diffraction spots similar to single crystal revealed that the cell boundaries are low-angle grain boundaries with a misorientation angle of several degrees (like ~5.64° in the insert of Fig. 6(a)). Moreover, there are high-density dislocations tangled inside the cells as pointed by the green arrow in Fig. 6(a). With increasing the ARB cycle to 3, the dislocation cells gradually disappear in Al layers, and some equiaxed clear grains without dislocations inside are formed in dislocations pile-up areas of Al layers due to recrystallization, as pointed by blue arrows in Fig. 6(b). When the ARB cycle is 6 and 8 (Fig. 6(c)–(e)), most of the grains in the Al layers are equiaxed and recrystallized, as pointed by blue arrows, and there are no dislocations accumulated in them. However, no evident recrystallized grains are found in Cu layers even when the ARB cycle is 6 or 8, as displayed in Fig. 6(d)–(f). Moreover, strip-like grains with the thickness of about 164.87 nm and large numbers of tangled dislocations at the interior are found in Cu layers, as presented in Fig. 6(e)–(f). It should be pointed out that the three cavities in Fig. 6(e) are formed during the ion milling of TEM samples, rather than formed at

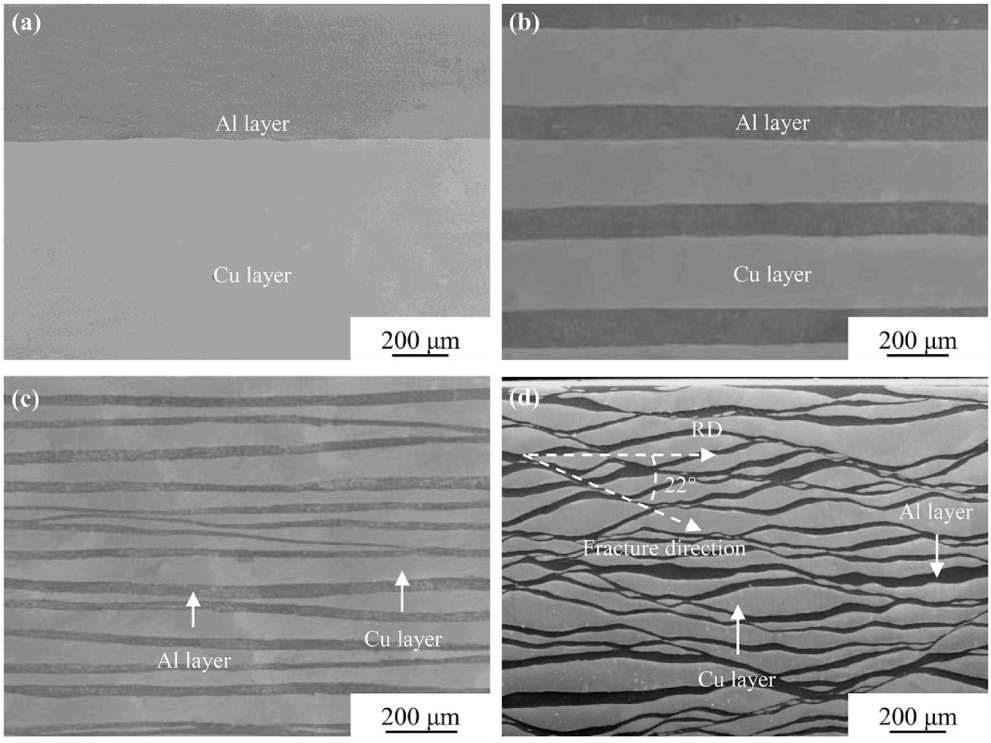


**Fig. 2.** FIB/SEM images for microscopic morphologies of Al and Cu layers with various ARB cycles.

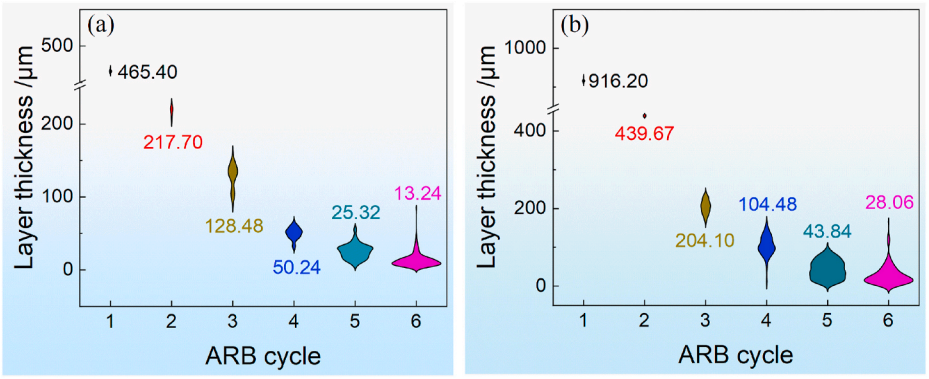


**Fig. 3.** Quantitative statistics of Al (a) and Cu (b) layer thickness versus ARB cycle. The layer thickness values in the figures are calculated by the weighted average method, and the sides are statistical distributions of layer thickness.

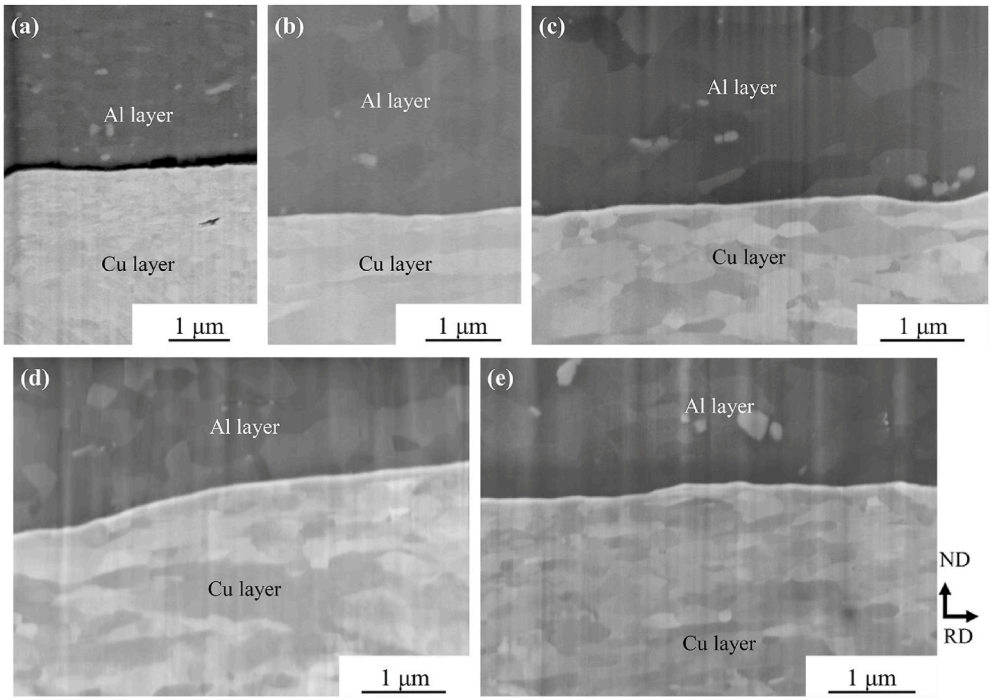


**Fig. 4.** FIB/SEM images for Al/Cu interfaces of Al/Cu laminated composites with various ARB cycles: (a) 1, (b)–(c) 3, (d)–(e) 6. (b) and (d) are SEM images at the center of ND-RD plane, (c) and (e) are SEM images near the edge of ND-RD plane.

the Al/Cu metallurgical interface during the ARB process.

The different microstructure evolutions of Al and Cu layers during ARB process can be explained from their different melting points and stacking faults energies (SFEs). Usually, the recrystallization temperature is 0.4 times of the melting point, calculated in Kelvin (K). Melting points for Al and Cu are about 933.15 K and 1356.15 K, respectively. Then the calculated recrystallization temperatures of Al and Cu are about 373.26 K (100.11 °C) and 542.46 K (269.31 °C), respectively. Therefore, the deformation heat induced by ARB tends to activate recrystallization in Al layers rather than in Cu layers [28]. Besides, SFEs for Al and Cu are 146 mJ $m^{-2}$ [29] and 44.4 mJ $m^{-2}$ [30], respectively. For crystals with low SFEs, such as Cu, super-dislocations can easily dissociate into partial dislocations bounded by stacking fault ribbons. In such a case to reduce the dislocation density, grain boundaries directly bulge from low dislocation density regions into high dislocation density regions. Consequently, equiaxed DRX grains are formed (termed as "Discontinuous DRX") [31]. However, for crystals with high SFEs, the dissociation is hampered, causing serious dislocations pile-ups. Thereupon, to relieve dislocations pile-ups, dislocations climb to form sub-grains. Finally, sub-grains are transformed into equiaxed DRX grains (termed as "Continuous DRX") [32]. The rate for dislocations climbing is faster than that for grain boundaries bulging, hence recrystallized grains with the equiaxed shape are intensively formed in Al layers with high SFE.

Fig. 7 presents the grain size distribution histograms of Al layers in the ARB-processed Al/Cu laminated composites. For elongated grains or dislocation cells in Fig. 5(a), one just measured the grain thickness value due to the large aspect ratio. For equiaxed grains in Fig. 5(e), the average grain diameter measured in different directions was adopted as grain size using Image-Pro Plus software. As seen from Fig. 7, when the ARB cycle is 1, the grain thickness of Al layers varies from 0.18 μm to 1.15 μm, and the average value is about 0.65 μm, indicating a large difference in Al grain size. When the ARB cycle is 3, the maximum and minimum values of Al grain size are 0.98 μm and 0.07 μm, respectively. And the average grain size is about 0.43 μm. When the ARB cycle further increases to 6, the Al grain size changes in the range of 0.05–0.64 μm and the average value of about 0.28 μm. Although the variation range of Al grain size is different, the measured grain size data follow a normal

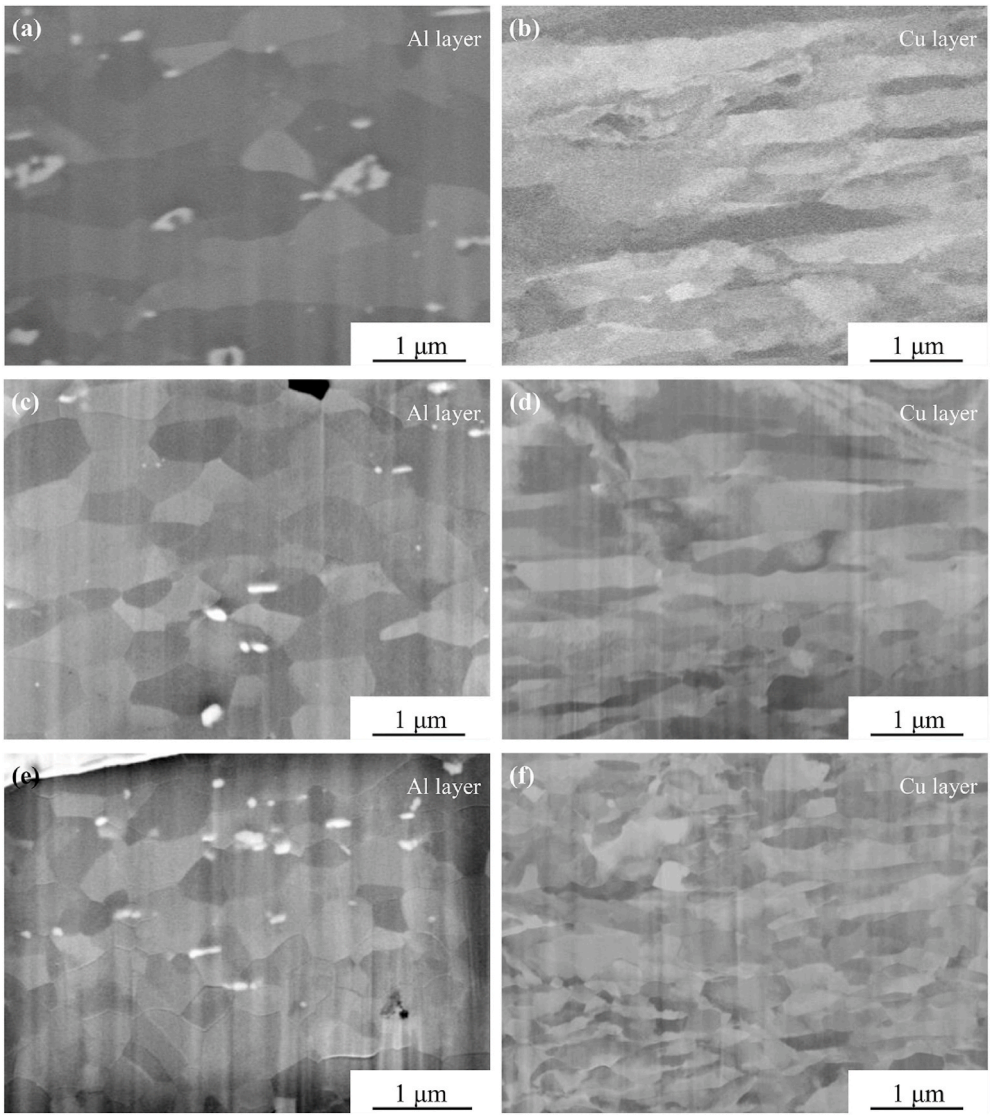


**Fig. 5.** FIB/SEM images of Al/Cu laminated composites with various ARB cycles: (a)–(b) 1, (c)–(d) 3, (e)–(f) 6. (a), (c) and (e) are microstructure of Al layers, (b), (d) and (f) are microstructure of Cu layers. The horizontal direction in Fig. 5 is the same as that in Fig. 2.

distribution.

### 3.2. Mechanical properties of Al/Cu laminated composites

Fig. 8 shows the Vickers micro-hardness of Al/Cu laminated composites ARB-processed with various cycles. As seen from Fig. 8, the micro-hardness values of the initial Al and Cu layers before ARB are 35.92 HV and 50.88 HV, respectively. The first cycle of ARB deformation increases the micro-hardness values of Al and Cu layers sharply and significantly to 46.81 HV and 114.74 HV, respectively. The further ARB processes only enhanced the micro-hardness slightly to saturated values of 48.13 HV and 127.53 HV, respectively. During the whole ARB process, the micro-hardness of Al layers is always much lower than that of Cu layers.

In literature, there are two reasons for the hardening of ARB-processed Al/Cu laminated composites. The first is that new phases (like AlCu or $Al_2Cu$ [33,34]) might form at the Al/Cu interface during ARB. However, our EDS results in Fig. 9(a)-(b) indicate that there are no new phases formed at the Al/Cu interface. Herewith, the enhanced micro-hardness in the Al or Cu layers is mainly connected to the ARB cycle (strain). During the subsequent ARB process, the dislocation cells in the Al layers were gradually transformed into recrystallized grain structure, and the dislocations in the Cu layers were gradually saturated, causing the slow increase in micro-hardness.

Uniaxial tensile experiments were adopted to characterize tensile properties of ARB-processed Al/Cu laminated composites. Fig. 10(a) presents engineering stress-strain curves of Al/Cu laminated composites with 1–8 ARB cycles. Fig. 10(b) and Table 1 show the corresponding ultimate strength ($\sigma_{us}$), uniform elongation ($e_u$) and elongation to failure ($e_f$) extracted from Fig. 10(a). As seen from Fig. 10(a)–(b), the values of $\sigma_{us}$, $e_u$ and $e_f$ of Al/Cu laminated composites with 1 ARB cycle are 279.20 MPa, 1.25% and 6.91%, respectively. ARB for 3 cycles enhanced the ultimate strength and uniform elongation to 324.51 MPa and 1.71% by keeping the ductility unchanged at 6.66%, and further ARB for 4 cycles increased the ultimate strength up to 358.71 MPa while kept the uniform elongation as 1.43% and decreased the ductility to about 3.35%. The elongation to failure of the ARB-processed Al/Cu laminated composites significantly decreases, and the ultimate strength decreases slightly as the ARB cycle increase from 4 to 8. This demonstrates that brittle fracture occurs in the Al/Cu laminated composites with high ARB cycles [35]. It is ascribed to the incompleteness of Al and Cu layers (invalid "brick-and-mortar" structure), as revealed in Fig. 2(d) and Fig. 9 (b). For all ARB-processed samples, pre-mature necking without evident strain hardening occurred immediately after yielding, and this is a

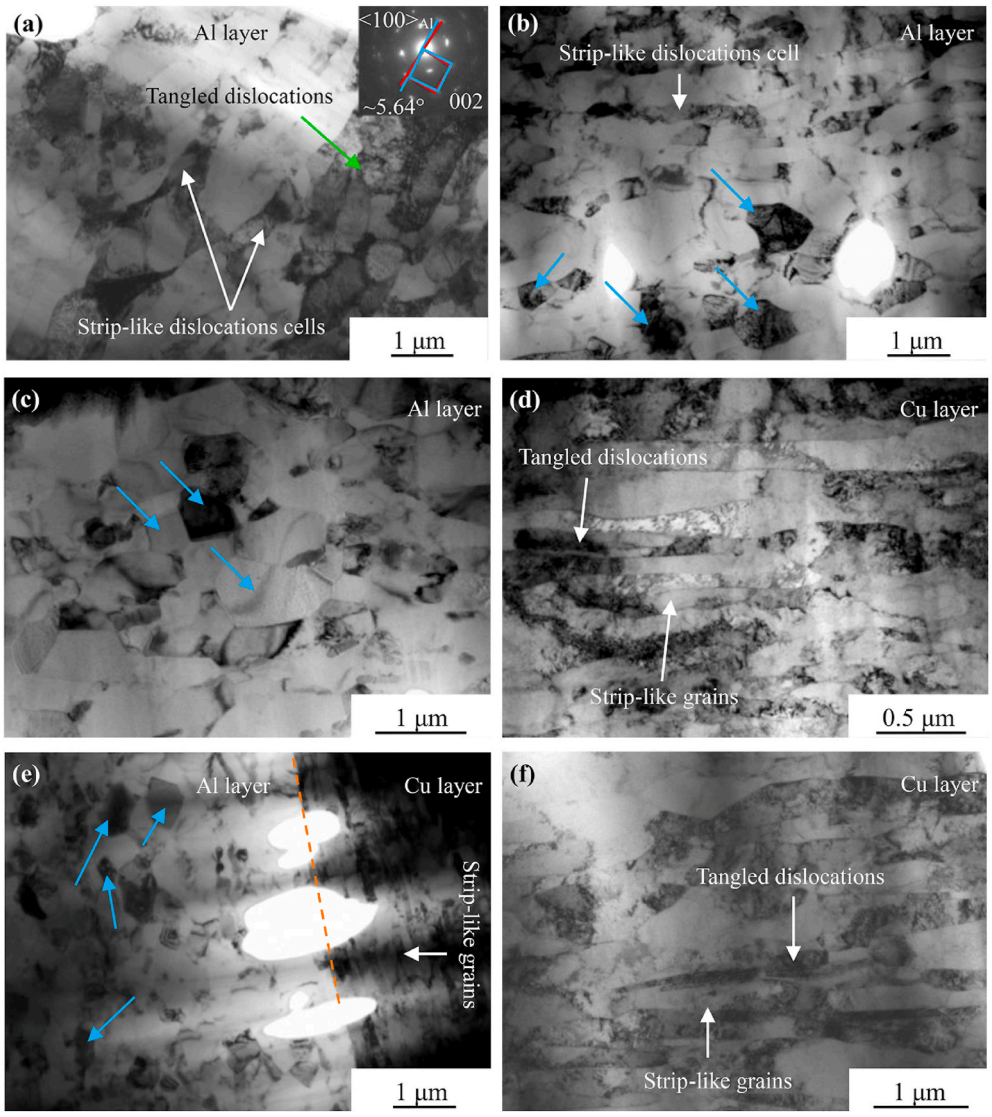


**Fig. 6.** Bright-field TEM images of Al/Cu laminated composites with various ARB cycles: (a) 1, (b) 3, (c)–(d) 6, (e)–(f) 8. (a)–(c) are Al layers, (d) and (f) are Cu layers, (e) is the Al/Cu interface. The insert in (a) is the selected area electron diffraction (SAED) pattern in the dotted circle. The blue arrows indicate recrystallized grains. (For interpretation of the references to colour in this figure legend, the reader is referred to the Web version of this article.)

typical result for the severely deformed metals. The initial ARB process caused nearly saturated dislocations densities in both Al and Cu layers (Fig. 6(a) and (d)), which makes follow-up dislocations difficult to slip and accumulate during tensile tests. The recovery and recrystallization in Al layers as well as the reliable Al/Cu metallurgical bonding interface slightly regains uniform elongation during subsequent ARB process. Howbeit, there is still no much space for dislocations accumulation in the ultrafine-grained Al layers, and therefore the enhancement of uniform elongation was very tiny and limited.

Fig. 11 presents tensile fracture surfaces of the ARB-processed Al/Cu laminated composites. As seen from Fig. 11(a)–(d), the interfacial bonding quality of pre-formed Al/Cu interface (at top and bottom positions) is better than that of newly-formed Al/Cu interface (pointed by red arrows in Fig. 11). The pre-formed bonding interface is hard to distinguish at ARB cycles of 6–8 (Fig. 11(c)–(d)). According to engineering stress-strain curves (Fig. 10), ductile fracture occurs during tensile tests of Al/Cu laminated composites with low ARB cycles, and brittle fracture occurs in those with high cycles. Fig. 11(e)–(f) show tensile fracture surfaces of Al and Cu layers for the Al/Cu laminated composite with 1 ARB cycle. Intensive dimples are observed in Fig. 11(e), indicating that ductile fracture occurs in Al layers. Tearing ridges and dimples are observed in Fig. 11(f), implying that both ductile and brittle fracture occurs in the corresponding Cu layers. The brittle martensite and intermetallic compounds also exhibit ductile fracture and contribute more toughness when they are embedded in a soft laminated material [36–39]. The Al/Cu laminated composite with 1 ARB cycle presents a notable ductile fracture characteristic, which is related to the synchronous plastic flow in Al and Cu layers. For the Al/Cu laminated composite with 8 ARB cycles, massive dimples are observed in Al layers (Fig. 11(g)), meaning that ductile fracture occurs in Al layers. Meanwhile, Cu layers present a serious lamellar tearing fracture surface (Fig. 11(h)), indicating that brittle fracture happens in Cu layers. These observations agree well with the brittle-like fracture of the Al/Cu laminated composites with high ARB cycles.

As displayed in Fig. 2(d), many Al/Cu interfaces are newly formed in Al/Cu laminated composites with high ARB cycles. Considering that these interfaces are not parallel to the loading direction, quite a lot of tensile cracks are easily initiated in these positions during later tensile tests. Besides, a certain number of cracks have been introduced into Cu layers near the Al/Cu interfaces, which would severely aggravate cracks propagation during later tensile tests. Hence lamellar tearing morphology could be found in Cu layers ARB-processed with high ARB

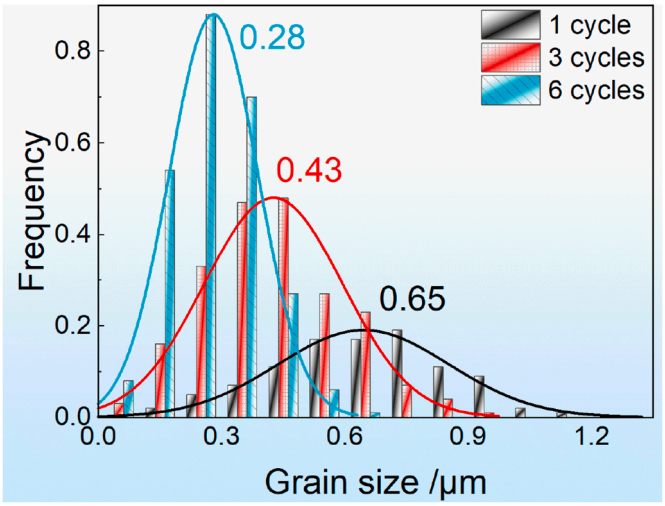


**Fig. 7.** Grain size distribution histograms of Al layers in Al/Cu laminated composites with 1, 3 and 6 ARB cycles. The values present the average grain size and the simulated curves follow normal distributions. For the elongated grains or dislocation cells in sample with 1 ARB cycle, the grain thickness value is just measured due to large aspect ratio.

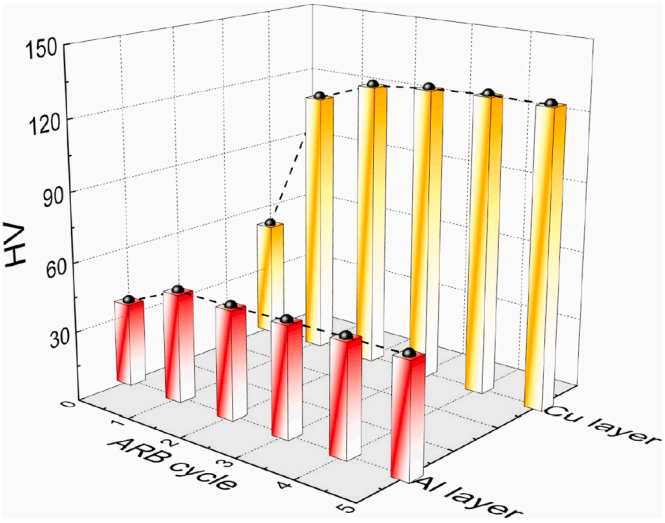


**Fig. 8.** Micro-hardness changes of Al/Cu laminated composites versus ARB cycle.

cycles.

### 3.3. Microstructure of Al/Cu laminated composites after ARB + intermediate annealing

In this part, microscopic morphologies of Al/Cu laminated composites after ARB + intermediate annealing were investigated to clarify the influence of intermediate annealing, as displayed in Fig. 12. Fig. 13 presents the effect of ARB cycle on Al and Cu layers thicknesses of ARB + intermediate annealing processed Al/Cu laminated composites. One thing should be pointed out is that the Al/Cu laminated composites after 1–2 ARB + intermediate annealing cycles are the same as that after 1–2 direct ARB cycles, because no intermediate annealing was carried out on the Al/Cu laminated composites. So do the microstructure and mechanical properties of Al/Cu laminated composites after 1–2 ARB + intermediate annealing cycles. As seen from Fig. 12(a)–(c), both the thicknesses of Al and Cu layers after ARB + intermediate annealing decrease with increasing ARB cycle, which is consistent with previous observations (Fig. 2(a)–(d)). By comparing Fig. 13 with Fig. 3, the thickness of Al layers after ARB + intermediate annealing is smaller than that of Al layers after ARB, so do Cu layers. Moreover, the layer thickness is more uniform after ARB + intermediate annealing, especially for Cu layers. The stacking layers in Fig. 12(a)–(b) are 4 and 16, respectively, proving that the relationship between layer numbers and the ARB cycle is a power function relationship with the cardinality of 2. Interestingly, Cu layers are sound and Al layers slightly undulate in Fig. 12(c). Such observations are quite different from the macroscopic morphology of Al/Cu laminated composites with the same ARB cycle in Fig. 2(d). From this, it was determined that the intermediate annealing alleviates severe inhomogeneity of strain distribution in Cu layers, and therefore improves the plasticity of Al/Cu laminated composites.

### 3.4. Mechanical properties of Al/Cu laminated composites after ARB + intermediate annealing and final annealing

Fig. 14 presents the Vickers micro-hardness of the Al/Cu laminated composites after ARB + intermediate annealing with various cycles. Both the micro-hardness of Al and Cu layers firstly decreases as the ARB cycle increases from 2 to 3, then slightly increases as the ARB cycle increases to 4, and finally marginally increases for Al layers and decreases for Cu layers (Fig. 14). The intermediate annealing was performed after every 2 cycles, which reduces the corresponding dislocations density in Al and Cu layers. Thus, the micro-hardness would decrease in Al and Cu layers with 3 or 5 ARB cycles. Compared with the micro-hardness in Fig. 8 without intermediate annealing, the corresponding micro-hardness values in Fig. 14 are slightly smaller due to annealing-induced recovery.

Fig. 15(a) shows engineering stress-strain curves for Al/Cu laminated composites ARB + intermediate annealing processed with 1–8 cycles.

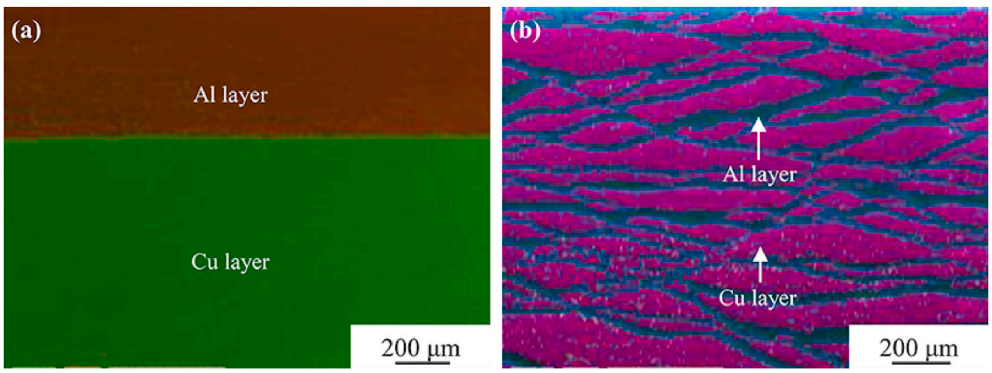


**Fig. 9.** Al and Cu map scanning images of Al/Cu laminated composites with various ARB cycles: (a) 1, (b) 6.

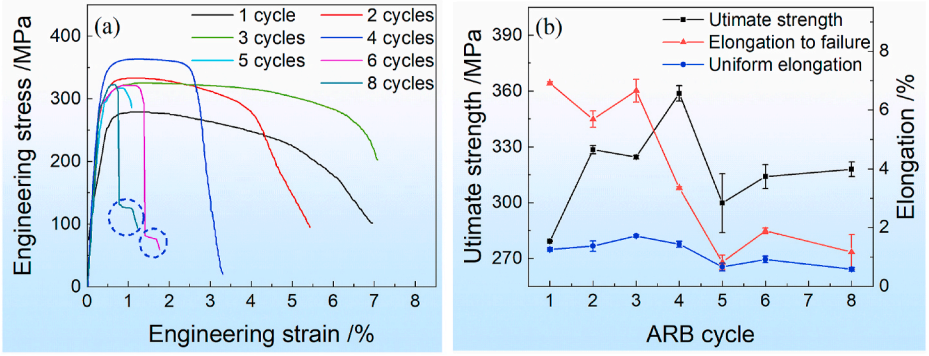


**Fig. 10.** (a) Engineering stress-strain curves and (b) tensile properties of Al/Cu laminated composites with various ARB cycles. The tensile tests were conducted at ambient temperature with a tensile rate of 0.5 mm $s^{-1}$.

**Table 1**
Tensile properties of Al/Cu laminated composites with various ARB cycles.

| Cycle number | 1 | 2 | 3 | 4 | 5 | 6 | 8 |
|---|---|---|---|---|---|---|---|
| Ultimate strength/MPa | 279.20 | 328.45 | 324.51 | 358.71 | 299.69 | 314.06 | 317.88 |
| Uniform elongation/% | 1.25 | 1.37 | 1.71 | 1.43 | 0.66 | 0.92 | 0.58 |
| Elongation to failure/% | 6.91 | 5.69 | 6.66 | 3.35 | 0.82 | 1.88 | 1.16 |

Fig. 15(b) and Table 2 show the corresponding ultimate strength ($\sigma_{us}$), uniform elongation ($e_u$) and elongation to failure ($e_f$) extracted from Fig. 15(a). As seen from Fig. 15(a)–(b) and Table 2, the tensile strength increases from 279.20 MPa to 461.97 MPa, and the elongation to failure decreases from 6.91% to 3.51% as the ARB + intermediate annealing cycle increases from 1 to 8. Compare with Fig. 10(a)–(b) and Fig. 15(a)-(b), both the tensile strength and elongation to failure of ARB + intermediate annealing processed Al/Cu laminated composites are significantly higher than the corresponding values of ARB-processed Al/Cu laminated composites. Undoubtedly the intermediate annealing is the main cause, which weakens the inhomogeneity of strain distribution and enhances plastic deformation and Al/Cu interface bonding quality via recovery and recrystallization.

Additionally, tensile tests were used to investigate the influence of final annealing. Fig. 15(c) presents engineering stress-strain curves of Al/Cu laminated composites fabricated via ARB + intermediate annealing with 6 cycles and final annealing at 300 °C. Fig. 15(d) and Table 3 show mechanical properties extracted from Fig. 15(c). As seen from Fig. 15(c)–(d) and Table 3, the tensile strength shows a decreased tendency, while the elongation to failure presents an increasing trend when the annealing time increases to 120 min. The minimum tensile strength is 214.42 MPa, and the maximum elongation to failure is 15.82% due to annealing-induced recrystallization. When the annealing time is 180 min, the ultimate strength increases to 283.62 MPa, and the elongation to failure decreases to 6.75%. XRD results revealed that some brittle intermetallics (like AlCu and $Al_2Cu$) are produced during final annealing, as present in Fig. 15(e). When the annealing time increases to 180 min, the volume fraction of brittle intermetallics increases, leading to the increase of tensile strength and the decrease of elongation to failure.

Moreover, the effect of final annealing on tensile fracture behaviors was investigated, and these fracture surfaces of Al/Cu laminated composites after ARB + intermediate annealing and final annealing were displayed in Fig. 16. For Al/Cu laminated composites without final annealing (Fig. 16(a)), the fracture surface exhibits patches of dimples, indicating the dominant fracture behavior is a typical ductile fracture. After final annealing with 30 min (Fig. 16(b)), some dimples and cracks are presented on the fracture surface, but few dimples can be found near the bonding interface. When the annealing time is 120 min, the Al layers necked into sharp lines, as pointed by yellow arrows in Fig. 16(c), resulting in the large ductility. When the annealing time is 180 min (Fig. 16(d)), the necked Al layers still can be distinguished (yellow arrows), while Cu layers show tearing ridges and dimples (pointed by white arrows). This suggests that the fracture type switches from ductile fracture to less ductile fracture as the annealing time increases. Combining with Fig. 15(e), the transition of fracture behavior might be associated with the formation of brittle intermetallics.

## 4. Discussions

### 4.1. Morphology evolutions of ARB-processed Al/Cu laminated composites

According to the above results in Figs. 2–7, Al and Cu layers present a notable difference in microstructure and morphology evolutions during the ARB process. Wu et al. [38] found that the interface constraint is decisive to the change of deformation behavior in brittle/ductile laminated composites. In the present work, the interface constraint might be the main cause for the notable difference in Al and Cu layers. Considering that activated slip systems of Al are close to that of Cu due to their same crystal structures (face-centered cubic lattices), the plastic flow of Cu layers could keep pace with that of Al layers at the initial stage of ARB (Fig. 17(a)). Nevertheless, the slip systems activation in the hard Cu layers cannot synchronize with that in soft Al layers, and this situation would be more striking with the increasing of strain (ARB cycle). So, the plastic flow of Al layers is partly limited by the reliable metallurgical bonding of Al/Cu interfaces. This means that Al grains near Al/Cu interfaces are subjected to compressive stress along the Al/Cu interface, which improves the plasticity of Al layers; Cu grains near the Al/Cu interface are subjected to tensile stress along the Al/Cu interface, which is detrimental to the ductility of Cu layers. To a certain extent of deformation, flow instability like crack would occur in the Cu layers near the surface, as illustrated in Fig. 17(b). With the proceeding of ARB, Cu layers would fracture, and Al layers with high plasticity would gradually immigrate into cracks when the Al/Cu laminated composites were ARB processed at lower strain rates (Figs. 2(d) and Fig. 17(c)).

### 4.2. Relationships between microstructure and tensile properties of ARB-processed Al/Cu laminated composites

Compare with the previous work [40], the ductility (6.91%) of ARB-processed Al/Cu laminated composites is higher than that (5.40%)

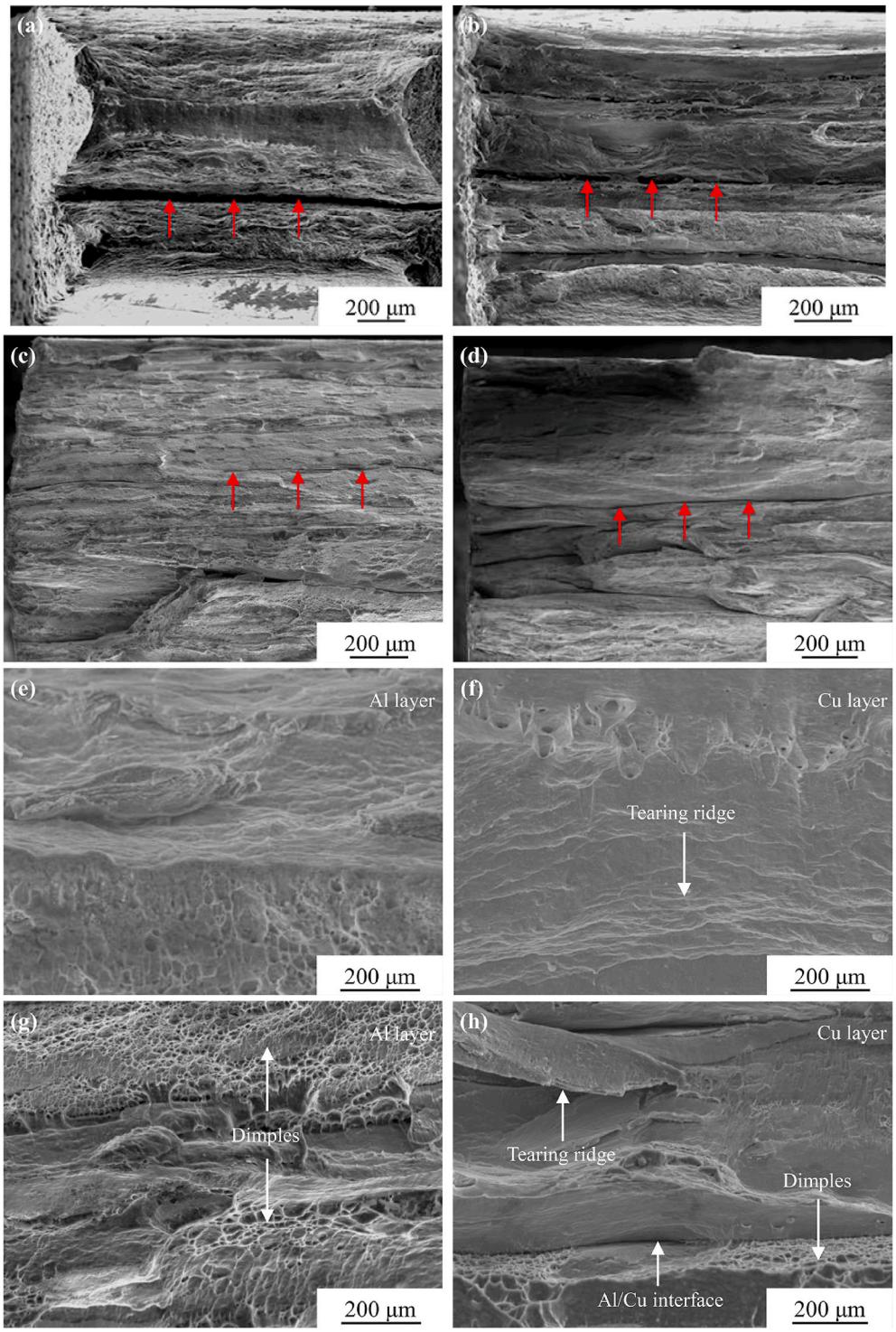


**Fig. 11.** Fracture surfaces of the Al/Cu laminated composites with various ARB cycles: (a) 1, (b) 3, (c) 6, (d) 8. Fracture surfaces of Al layer (e) and Cu layer (f) with 1 ARB cycle. Fracture surfaces near Al layer (g) and Cu layer (h) with 8 ARB cycles. The red arrows indicate the newly-formed Al/Cu interface. (For interpretation of the references to colour in this figure legend, the reader is referred to the Web version of this article.)

of ARB-processed Cu with 1 ARB cycles. So does the ductility with 3 ARB cycles. Ti/Al laminated composite has been reported to have excellent tensile ductility, overwhelmingly surpassing its constituents Ti and Al due to delocalization of plastic strain and prevention of premature necking instability from the laminated structure [11]. Detailed *in situ* experimental observation under loading indicated that the significantly increased ductility originates from the significantly enhanced stress/-strain transferring ability by laminated Ti/Al structure [11].

The synchronous plastic flow is achieved in Al and Cu layers when Al/Cu laminated composites ARB-processed with 1–3 cycles (Fig. 2(a)–(b)). At this time the ARB-introduced dislocations and Al/Cu metallurgical interfacial bonding are beneficial to tensile properties improvement (Fig. 10(b)). The reliable interfacial bonding also brings significant interface constraint, which delays the yielding and improves the yielding strength [41]. However, the plastic flow of Cu layers is gradually out of synchronization with that of Al layers when increasing the

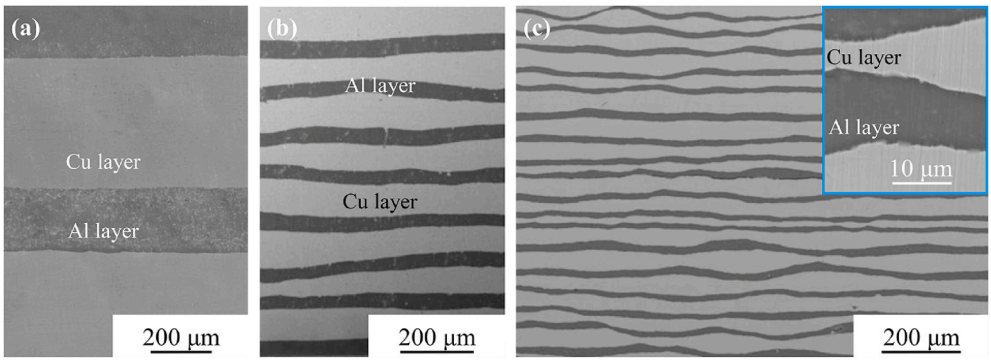


**Fig. 12.** Microscopic morphologies of Al/Cu laminated composites with various ARB + intermediate annealing cycles: (a) 2, (b) 4, (c) 6. Note that the intermediate annealing was performed after every 2 cycles. In other words, no intermediate annealing was performed on Al/Cu laminated composites in (a). The insert is a magnification of (c).

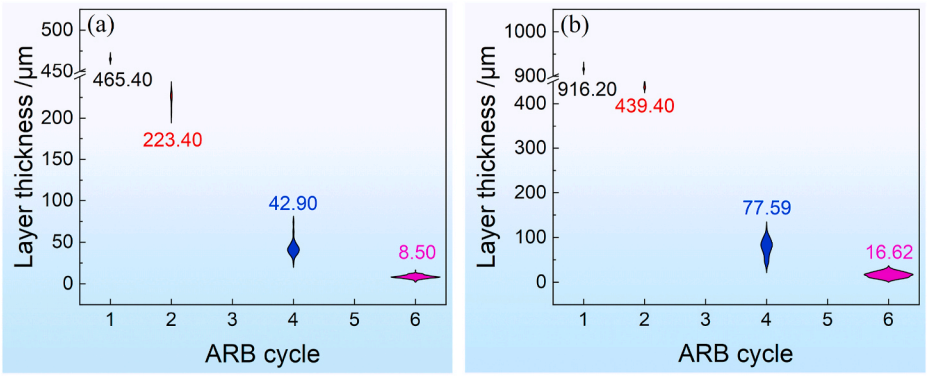


**Fig. 13.** Quantitative statistics of Al (a) and Cu (b) layer thickness versus ARB + intermediate annealing cycle. The layer thickness values are calculated in the same way as that in Fig. 3, and the sides are the same as that in Fig. 3.

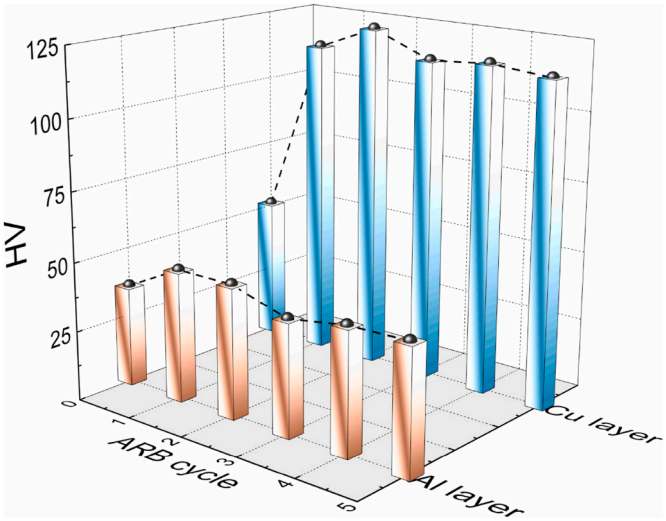


**Fig. 14.** Micro-hardness changes of the Al/Cu laminated composites versus ARB + intermediate annealing cycle. Note that the micro-hardness of Al/Cu laminated composites with 1 and 2 ARB + intermediate annealing cycles are same as the corresponding values of Al/Cu laminated composites with same ARB cycles, because the intermediate annealing was performed after every 2 ARB cycles.

ARB cycles to 4, which is manifested as the large variation of Cu layer thickness. According to Fig. 3, the minimum and maximum of corresponding Cu layers are 12 μm and 159 μm, respectively. Combine with Fig. 10(b), it can be reasonably concluded that the non-uniform of Cu layers thickness is the main cause for the decrease of uniform elongation and elongation to failure as the ARB cycle increases from 3 to 4. Nevertheless, the ultimate strength continues to increase up to 358.71 MPa for the continuity is still maintained in Cu layers. However, the asynchronous plastic flow brings many micro-cracks at the Cu layer interfaces (illustrated in Fig. 17(c)) when increasing the ARB cycle from 4 to 5, which severely deteriorate the ultimate strength and elongation to failure in Fig. 10(a)–(b). Huang et al. [42] also acclaimed that the formation of cracks in hard Ti layers instead of at the bonding interface or in soft Al layers seriously damage the tensile ductility of interface-sound Ti/Al laminated composites. With the proceeding of ARB with cycles larger than 5, some Cu layers are fragmented, introducing more Al/Cu interfaces in ARB-processed Al/Cu laminated composites. Additionally, some Al layers merge with others to form tilt layers (Fig. 2(d)). To a small tensile strain, the introduced Al/Cu interfaces can retard dislocations movements and increase the ultimate strength. Also, these tilt Al layers are conducive to the dislocations movements, which seriously damage the ultimate strength and elongation to failure of ARB-processed Al/Cu laminated composites with 6–8 ARB cycles in Fig. 10(a). At the later tensile stage, the Cu layers which are mainly bearing tensile load, are fractured, causing the dramatic drop of the tensile curves, as shown in dotted circles of Fig. 10(a). The unbroken Al layers more or less improved the ductility by about 0.5% till the final fracture. Coincidentally, similar results can be found during loading of nacre in nature. Strong and tough nacre is a typical laminated biological material with alternately stacked "brick-and-mortar" structure. The $CaCO_3$ mineral bricks (aragonite) provide strength and organic mortars (protein) endow toughness [43]. Under loading, the shear between aragonite platelets would introduce enough inelastic deformation

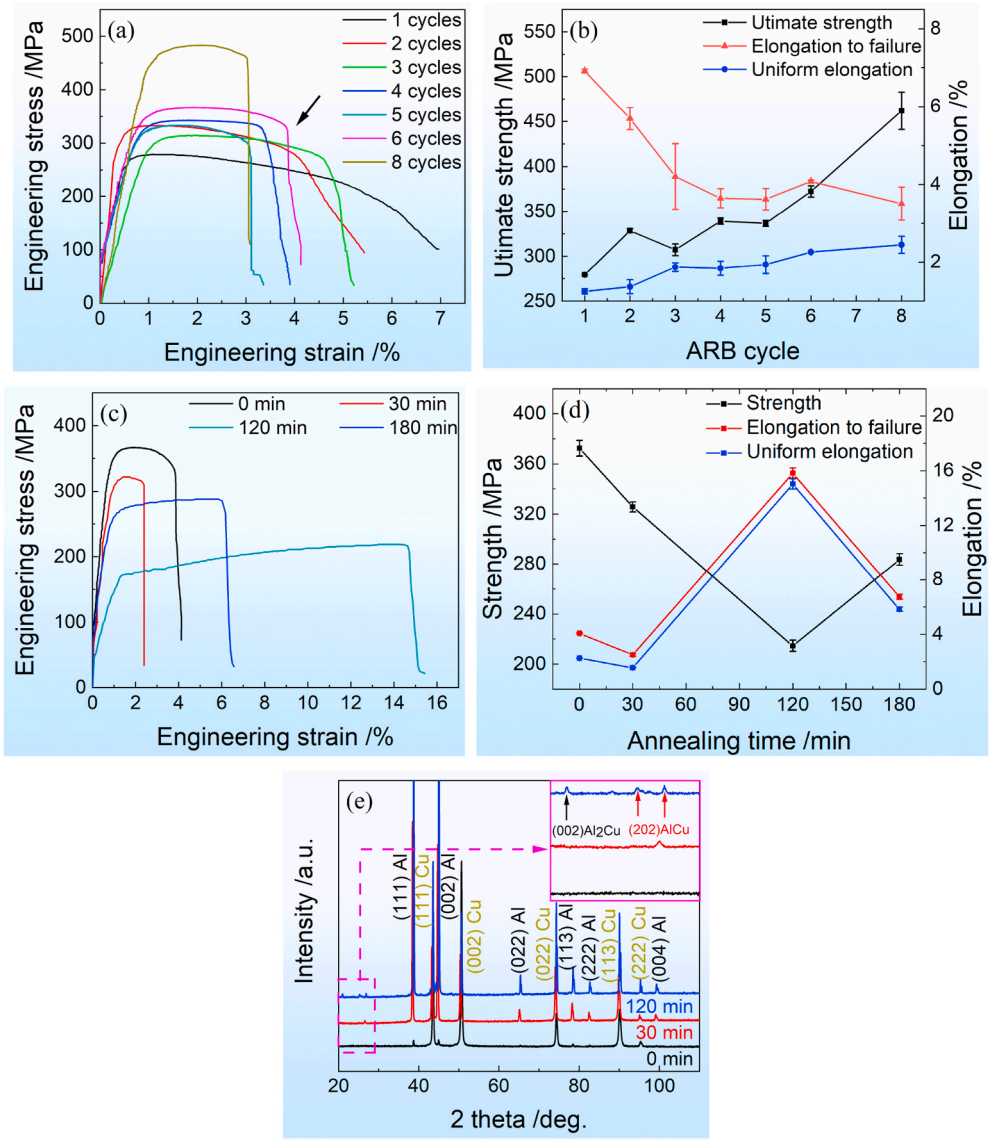


**Fig. 15.** (a) Engineering stress-strain curves and (b) mechanical properties of the Al/Cu laminated composites with various ARB + intermediate annealing cycles, (c) Engineering stress-strain curves, (d) mechanical properties and (e) XRD patterns of the Al/Cu laminated composites with 6 ARB + intermediate annealing cycles and finally annealed at 300 °C with various times. The curves in (a) with 1 and 2 cycles are same as the curves in Fig. 10(a) with same cycles.

**Table 2**
Tensile properties of Al/Cu laminated composites with various ARB + intermediate annealing cycles.

| Cycle number | 1 | 2 | 3 | 4 | 5 | 6 | 8 |
|---|---|---|---|---|---|---|---|
| Ultimate strength/MPa | 279.20 | 328.45 | 307.29 | 339.17 | 336.61 | 372.38 | 461.97 |
| Uniform elongation/% | 1.25 | 1.37 | 1.87 | 1.84 | 1.94 | 2.26 | 2.45 |
| Elongation to failure/% | 6.91 | 5.69 | 4.21 | 3.65 | 3.62 | 4.08 | 3.51 |

**Table 3**
Tensile properties of Al/Cu laminated composites with 6 ARB + intermediate annealing cycles and finally annealed at 300 °C with various times.

| Annealing time/min | 0 | 30 | 120 | 180 |
|---|---|---|---|---|
| Ultimate strength/MPa | 372.38 | 325.59 | 214.42 | 283.62 |
| Uniform elongation/% | 2.26 | 1.55 | 15.02 | 5.83 |
| Elongation to failure/% | 4.08 | 2.50 | 15.82 | 6.75 |

in organic mortars, so that the strain can be redistributed and the toughness would be enhanced [44]. Moreover, the final "brick" pull-out and accompanied frictional sliding can also elevate the toughness further [5,45,46].

## 5. Conclusions

Al/Cu laminated composites were prepared via ARB with each rolling speed of 0.34 m $s^{-1}$ up to 8 cycles and/or intermediate annealing at 350 °C for 30 min as well as final annealing at 300 °C. The microstructure, mechanical properties and fracture morphologies were investigated. The main conclusions are as follows:

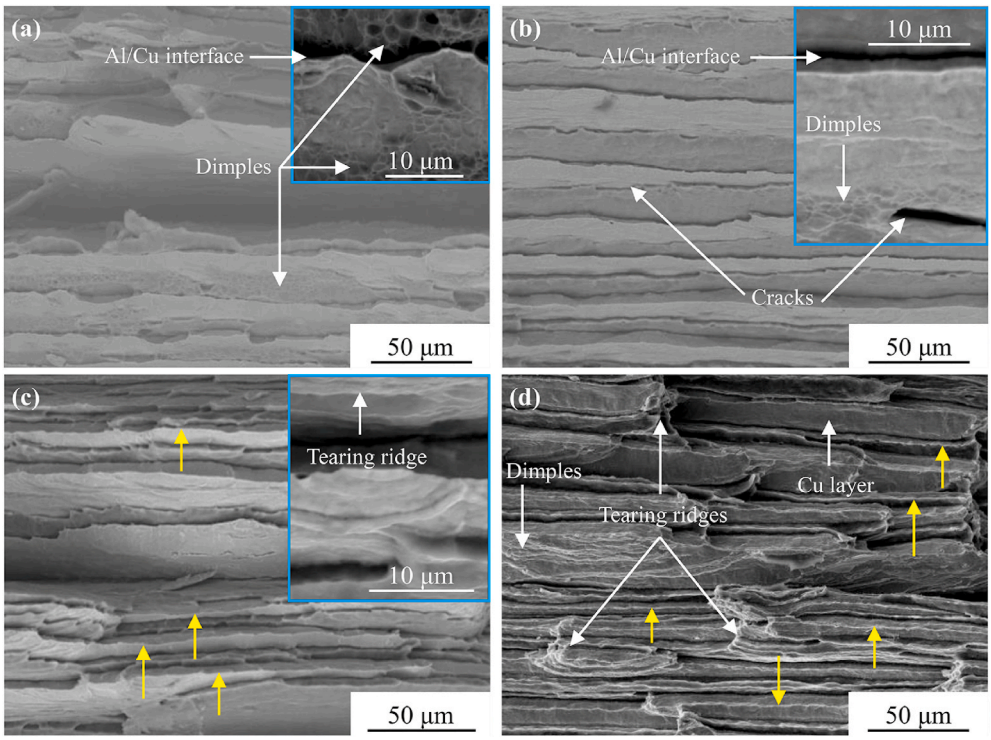


**Fig. 16.** Fracture surfaces of Al/Cu laminated composites with 6 ARB + intermediate annealing cycles and finally annealed at 300 °C with various times: (a) 0 min, (b) 30 min, (c) 120 min, (d) 180 min. The inserts are magnifications of corresponding fracture surfaces. Yellow arrows in (c) and (d) indicate the necked Al layers. (For interpretation of the references to colour in this figure legend, the reader is referred to the Web version of this article.)

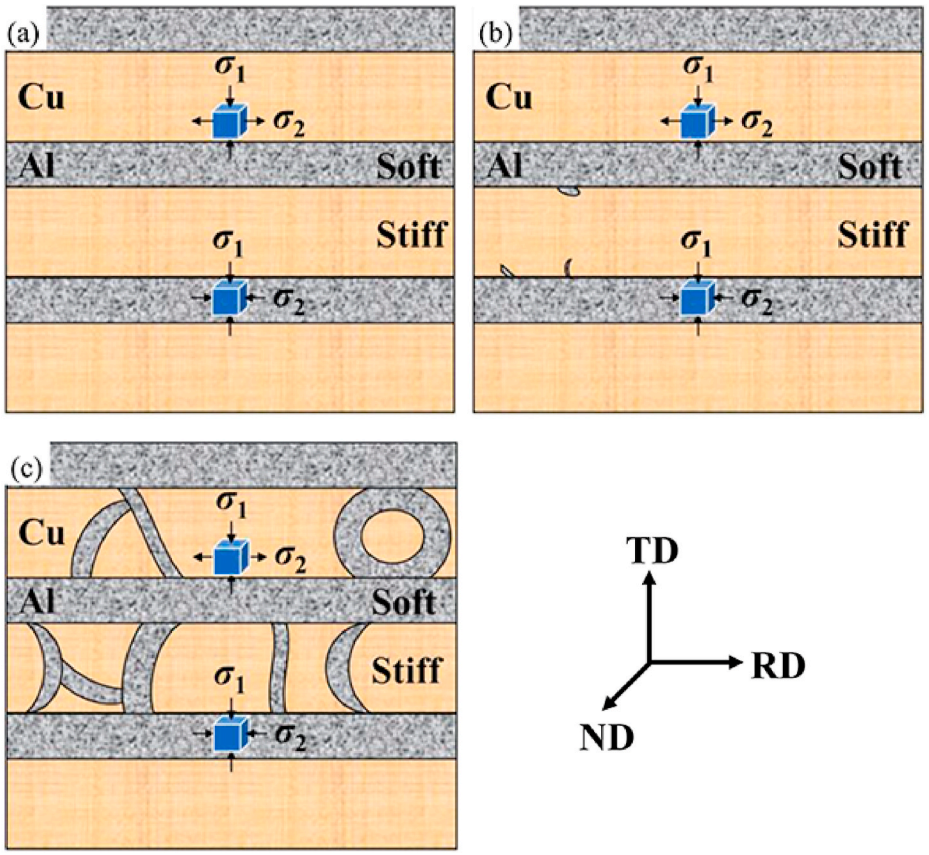


**Fig. 17.** Illustrations of microscopic morphology evolutions of Al and Cu layers during ARB: (a) sound Al and Cu layers at the initial ARB stage, (b) sound Al layers and cracked Cu layers at the middle ARB stage, (c) wavy-like Al layers and fractured Cu layers at the later ARB stage. The actual layer numbers are omitted in this illustration.

(1) When the ARB cycles increased from 1 to 6, the Al layer thickness decreased from 465.40 μm to 13.24 μm, and the Cu layer thickness decreased from 916.20 μm to 28.06 μm. Meanwhile, the equiaxed Al grain size decreased from 0.65 μm to 0.28 μm, while the strip-like Cu grain thickness decreased from 0.55 μm to 0.13 μm. Additionally, the ARB process enhanced the Al/Cu interface bonding quality.

(2) With increasing ARB cycles, both the micro-hardness of Al and Cu layers increased, while the tensile properties of Al/Cu laminated composites firstly increased and then decreased. The maximum tensile strength, uniform elongation and elongation to failure were 358.71 MPa, 1.71% and 6.91%, respectively. Intensive dimples were found on the fracture surface of Al layers, while massive tearing ridges were observed on the fracture surface of Cu layers. These variations of tensile properties are tightly linked to the layer-integrity and microstructures of Al and Cu layers.

(3) The intermediate annealing decreased the layer thickness and micro-hardness, but increased the thickness-uniformity of Al and Cu layers. The Al and Cu layer thicknesses in Al/Cu laminated composites prepared with 6 ARB + intermediate annealing cycles were 8.50 μm and 16.62 μm, respectively. And the micro-hardness of Al and Cu layers were 44.48 HV and 115.35 HV, respectively. Moreover, when the ARB + intermediate annealing cycle increased from 1 to 8, the tensile strength increased from 279.20 MPa to 461.97 MPa, whereas the elongation to failure decreased from 6.91% to 3.51%.

(4) As the final annealing time increased from 0 min to 120 min, the tensile strength of Al/Cu laminated composites with 6 ARB + intermediate annealing cycles decreased from 372.38 MPa to 214.42 MPa, and the elongation to failure increased from 4.08% to 15.82%. Further increasing the annealing time to 180 min enhanced the tensile strength and decreased the elongation to failure, which was related to the formation of brittle intermetallics.

## CRediT authorship contribution statement

**Runrun Xu:** Conceptualization, Data curation, Writing – original draft. **Ningning Liang:** Funding acquisition, Supervision. **Limin Zhuang:** Investigation, Data curation. **Dajie Wei:** Investigation, Data curation. **Yonghao Zhao:** Writing – review & editing, Funding acquisition, Supervision.

## Declaration of competing interest

The authors declare that they have no known competing financial interests or personal relationships that could have appeared to influence the work reported in this paper.

## Acknowledgments

This work was supported by the National Key R&D Program of China (Grant No. 2017YFA0204403), National Natural Science Foundation of China (Grant No. 51971112, 52071179 and 51225102), Natural Science Foundation of Jiangsu Province (BK20190478) and the Fundamental Research Funds for the Central Universities (Grant No. 30919011405 and 30920021160). The Jiangsu Key Laboratory of Advanced Nanomaterials and Technologies (SEM and TEM) is also acknowledged.

## References

[1] I.S. Lee, C.J. Hsu, C.F. Chen, N.J. Ho, P.W. Kao, Particle-reinforced aluminum matrix composites produced from powder mixtures via friction stir processing, Compos. Sci. Technol. 71 (2011) 693–698.

[2] Z.M. Zhang, Z. Li, Z.Q. Tan, H.T. Zhao, G.L. Fan, Y.J. Xu, D.B. Xiong, Z.Q. Li, Bioinspired hierarchical $Al_2O_3$/Al laminated composite fabricated by flake powder metallurgy, Compos. Part A-Appl. S. 140 (2021) 106187.

[3] S. Scudino, G. Liu, K.G. Prashanth, B. Bartusch, K.B. Surreddi, B.S. Murty, J. Eckert, Mechanical properties of Al-based metal matrix composites reinforced with Zr-based glassy particles produced by powder metallurgy, Acta Mater. 57 (2009) 2029–2039.

[4] M.E. Launey, E. Munch, D.H. Alsem, E. Saiz, A.P. Tomsia, R.O. Ritchie, A novel biomimetic approach to the design of high-performance ceramic/metal composites, J. R. Soc. Interface 7 (2010) 741–753.

[5] H. Bai, F. Walsh, B. Gludovatz, B. Delattre, C.L. Huang, Y. Chen, A.P. Tomsia, R. O. Ritchie, Bioinspired hydroxyapatite/poly(methyl methacrylate) composite with a nacre-mimetic architecture by a bidirectional freezing method, Adv. Mater. 28 (2016) 50–56.

[6] F. Liang, H.F. Tan, B. Zhang, G.P. Zhang, Maximizing necking-delayed fracture of sandwich-structured Ni/Cu/Ni composites, Scripta Mater. 134 (2017) 28–32.

[7] C. Ferraro, S. Meille, J. Réthoré, N. Ni, J. Chevalier, E. Saiz, Strong and tough metal/ceramic micro-laminates, Acta Mater. 144 (2018) 202–215.

[8] C.X. Huang, Y.F. Wang, X.L. Ma, S. Yin, H.W. Höppel, M. Göken, X.L. Wu, H.J. Gao, Y.T. Zhu, Interface affected zone for optimal strength and ductility in heterogeneous laminate, Mater. Today 21 (2018) 713–719.

[9] M. Göken, H.W. Höppel, Tailoring nanostructured, graded, and particle-reinforced Al laminates by accumulative roll bonding, Adv. Mater. 23 (2011) 2663–2668.

[10] T. Koseki, J. Inoue, S. Nambu, Development of multilayer steels for improved combinations of high strength and high ductility, Mater. Trans. 55 (2014) 227–237.

[11] M. Huang, G.H. Fan, L. Geng, G.J. Cao, Y. Du, H. Wu, T.T. Zhang, H.J. Kang, T. M. Wang, G.H. Du, H.L. Xie, Revealing extraordinary tensile plasticity in layered Ti-Al metal composite, Sci. Rep-UK 6 (2016) 38461.

[12] N. Tsuji, Y. Saito, H. Utsunomiya, S. Tanigawa, Ultra-fine grained bulk steel produced by accumulative roll-bonding (ARB) process, Scripta Mater. 40 (1999) 795–800.

[13] R. Gao, M.M. Jin, F. Han, B.M. Wang, X.P. Wang, Q.F. Fang, Y.H. Dong, C. Sun, L. Shao, M.D. Li, J. Li, Superconducting Cu/Nb nanolaminate by coded accumulative roll bonding and its helium damage characteristics, Acta Mater. 197 (2020) 212–223.

[14] D.C. Camilo Magalhães, O.M. Cintho, J.B. Rubert, V.L. Sordi, A.M. Kliauga, The role of shear strain during accumulative roll-bonding of multilayered composite sheets: pattern formation, microstructure and texture evolution, Mater. Sci. Eng. A 796 (2020) 140055.

[15] N. Ye, X.P. Ren, J.H. Liang, Microstructure and mechanical properties of Ni/Ti/Al/Cu composite produced by accumulative roll bonding (ARB) at room temperature, J. Mater. Res. Technol. 9 (2020) 5524–5532.

[16] S. Pasebani, M.R. Toroghinejad, M. Hosseini, J. Szpunar, Textural evolution of nano-grained 70/30 brass produced by accumulative roll-bonding, Mater. Sci. Eng. A 527 (2010) 2050–2056.

[17] Y. Wang, Y. Liao, R.Z. Wu, N. Turakhodjaev, H.T. Chen, J.H. Zhang, M.L. Zhang, S. Mardonakulov, Microstructure and mechanical properties of ultra-lightweight Mg-Li-Al/Al-Li composite produced by accumulative roll bonding at ambient temperature, Mater. Sci. Eng. A 787 (2020) 139494.

[18] M. Eizadjou, A. Kazemi Talachi, H. Danesh Manesh, H. Shakur Shahabi, K. Janghorban, Investigation of structure and mechanical properties of multi-layered Al/Cu composite produced by accumulative roll bonding (ARB) process, Compos. Sci. Technol. 68 (9) (2008) 2003–2009.

[19] L. Wang, Q.L. Du, C. Li, X.H. Cui, X. Zhao, H.L. Yu, Enhanced mechanical properties of lamellar Cu/Al composites processed via high-temperature accumulative roll bonding, T. Nonferr. Metal. Soc. 29 (2019) 1621–1630.

[20] T.B. Yu, Y. Du, G.H. Fan, R.Q. Xu, R. Barabash, N. Hansen, X.X. Huang, Y.B. Zhang, In-situ synchrotron X-ray micro-diffraction investigation of ultra-low-strain deformation microstructure in laminated Ti-Al composites, Acta Mater. 202 (2021) 149–158.

[21] V. Yousefi Mehr, M.R. Toroghinejad, A. Rezaeian, H. Asgari, J.A. Szpunar, A texture study of nanostructured Al–Cu multi-layered composite manufactured via the accumulative roll bonding (ARB), J. Mater. Res. Technol. 14 (2021) 2909–2919.

[22] V. Yousefi Mehr, M.R. Toroghinejad, A. Rezaeian, Mechanical properties and microstructure evolutions of multilayered Al-Cu composites produced by accumulative roll bonding process and subsequent annealing, Mater. Sci. Eng. A 601 (2014) 40–47.

[23] C.P. You, W.B. Xie, S. Miao, T.X. Liang, L.F. Zeng, X.H. Zhang, H. Wang, High strength, high electrical conductivity and thermally stable bulk Cu/Ag nanolayered composites prepared by cross accumulative roll bonding, Mater. Des. 200 (2021) 109455.

[24] C.C. Hsieh, M.S. Shi, W.T. Wu, Growth of intermetallic phases in Al/Cu composites at various annealing temperatures during the ARB process, Met. Mater. Int. 18 (2012) 1–6.

[25] M. Tayyebi, D. Rahmatabadi, A. Karimi, M. Adhami, R. Hashemi, Investigation of annealing treatment on the interfacial and mechanical properties of Al5052/Cu multilayered composites subjected to ARB process, J. Alloys Compd. 871 (2021) 159513.

[26] Y. Xiao, H. Besharatloo, B. Gan, X. Maeder, R. Spolenak, J.M. Wheeler, Combinatorial investigation of Al-Cu intermetallics using small-scale mechanical testing, J. Alloys Compd. 822 (2020) 153536.

[27] K. Liu, H.C. Yu, X. Li, S.J. Wu, Study on diffusion characteristics of Al-Cu systems and mechanical properties of intermetallics, J. Alloys Compd. 874 (2021) 159831.

[28] R.R. Xu, H. Li, M.Q. Li, Flow softening mechanism in isothermal compression of β-solidifying γ-TiAl alloy, Mater. Des. 186 (2020) 108328.

[29] Y. Mishin, D. Farkas, M.J. Mehl, D.A. Papaconstantopoulos, Interatomic potentials for monoatomic metals from experimental data and ab initio calculations, Phys. Rev. B 59 (1999) 3393–3407.
[30] Y. Mishin, M.J. Mehl, D.A. Papaconstantopoulos, A.F. Voter, J.D. Kress, Structural stability and lattice defects in copper: Ab initio, tight-binding, and embedded-atom calculations, Phys. Rev. B 63 (2001) 224106.
[31] R.R. Xu, H. Li, M.Q. Li, Dynamic recrystallization mechanism of γ and α phases during the isothermal compression of γ-TiAl alloy with duplex structure, J. Alloys Compd. 844 (2020) 156089.
[32] N. Cui, F.T. Kong, X.P. Wang, Y.Y. Chen, H.T. Zhou, Hot deformation behavior and dynamic recrystallization of a β-solidifying TiAl alloy, Mater. Sci. Eng. A 652 (2016) 231–238.
[33] C.Y. Chen, W.S. Hwang, Effect of annealing on the interfacial structure of aluminum-copper joints, Mater. Trans. 48 (2007) 1938–1947.
[34] J.D. Wilde, L. Froyen, S. Rex, Coupled two-phase [α(Al)+θ($Al_2Cu$)] planar growth and destabilisation along the univariant eutectic reaction in Al-Cu-Ag alloys, Scripta Mater. 51 (2004) 533–538.
[35] A. Hasnaoui, H. Van Swygenhoven, P.M. Derlet, Dimples on nanocrystalline fracture surfaces as evidence for shear plane formation, Science 300 (2003) 1550–1552.
[36] L. Geng, H. Wu, X.P. Cui, G.H. Fan, Recent progress on the fabrication of TiAl-based composites sheet by reaction annealing of elemental foils, Acta Metall. Sin. 54 (2018) 1625–1636.
[37] H. Wu, G.H. Fan, M. Huang, L. Geng, X.P. Cui, R.C. Chen, G.Y. Peng, Fracture behavior and strain evolution of laminated composites, Compos. Struct. 163 (2017) 123–128.
[38] H. Wu, G.H. Fan, M. Huang, L. Geng, X.P. Cui, H.L. Xie, Deformation behavior of brittle/ductile multilayered composites under interface constraint effect, Int. J. Plast. 89 (2017) 96–109.
[39] P. Lhuissier, J. Inoue, T. Koseki, Strain field in a brittle/ductile multilayered steel composite, Scripta Mater. 64 (2011) 970–973.
[40] X.R. Liu, L.M. Zhuang, Y.H. Zhao, Microstructure and mechanical properties of ultrafine-grained copper by accumulative roll bonding and subsequent annealing, Materials 13 (22) (2020) 5171.
[41] D.Y. Li, G.H. Fan, X.X. Huang, D.J. Jensen, K.S. Miao, C. Xu, L. Geng, Y.B. Zhang, T. B. Yu, Enhanced strength in pure Ti via design of alternating coarse- and fine-grain layers, Acta Mater. 206 (2021) 116627.
[42] M. Huang, C. Xu, G.H. Fan, E. Maawad, W.M. Gan, L. Geng, F.X. Lin, G.Z. Tang, H. Wu, Y. Du, D.Y. Li, K.S. Miao, T.T. Zhang, X.S. Yang, Y.P. Xia, G.J. Cao, H. J. Kang, T.M. Wang, T.Q. Xiao, H.L. Xie, Role of layered structure in ductility improvement of layered Ti-Al metal composite, Acta Mater. 153 (2018) 235–249.
[43] L.B. Mao, H.L. Gao, H.B. Yao, L. Liu, H. Cölfen, G. Liu, S.M. Chen, S.K. Li, Y.X. Yan, Y.Y. Liu, S.H. Yu, Synthetic nacre by predesigned matrix-directed mineralization, Science 354 (2016) 107–110.
[44] U.G.K. Wegst, H. Bai, E. Saiz, A.P. Tomsia, R.O. Ritchie, Bioinspired structural materials, Nat. Mater. 14 (2015) 23–36.
[45] O. Kolednik, J. Predan, F.D. Fischer, P. Fratzl, Bioinspired design criteria for damage-resistant materials with periodically varying microstructure, Adv. Funct. Mater. 21 (2011) 3634–3641.
[46] H. Wu, B.C. Jin, L. Geng, G.H. Fan, X.P. Cui, M. Huang, R.M. Hicks, S. Nutt, Ductile-phase toughening in $TiB_w$/Ti-$Ti_3Al$ metallic-intermetallic laminate composites, Metall. Mater. Trans. A 46 (2015) 3803–3807.